Front. Chem. Sci. Eng. 2018, 12(3): 450–456
https://doi.org/10.1007/s11705-018-1735-6

RESEARCH ARTICLE

Laser ablation of block copolymers with hydrogen-bonded azobenzene derivatives

Jintang Huang[1], Youju Huang (✉)[1], Si Wu (✉)[1,2]

1 Max Planck Institute for Polymer Research, Ackermannweg 10, 55128 Mainz, Germany
2 Hefei National Laboratory for Physical Sciences at the Microscale, CAS Key Laboratory of Soft Matter Chemistry, Anhui Key Laboratory of Optoelectronic Science and Technology, Innovation Centre of Chemistry for Energy Materials, Department of Polymer Science and Engineering, University of Science and Technology of China, Hefei 230026, China

Abstract Supramolecular assemblies (PS-b-P4VP (AzoR)) are fabricated by hydrogen-bonding azobenzene derivatives (AzoR) to poly(4-vinyl pyridine) blocks of polystyrene-block-poly(4-vinyl pyridine) (PS-b-P4VP). PS-b-P4VP(AzoR) forms phase separated nanostructures with a period of ~75–105 nm. A second length scale structure with a period of 2 μm is fabricated on phase separated PS-b-P4VP(AzoR) by laser interference ablation. Both the concentration and the substituent of AzoR in PS-b-P4VP(AzoR) affect the laser ablation process. The laser ablation threshold of PS-b-P4VP(AzoR) decreases as the concentration of AzoR increases. In PS-b-P4VP(AzoR) with different substituents (R = CN, H, and CH_3), ablation thresholds follow the trend: PS-b-P4VP(AzoCN) < PS-b-P4VP(AzoCH_3) < PS-b-P4VP(AzoH). This result indicates that the electron donor group (CH_3) and the electron acceptor group (CN) can lower the ablation threshold of PS-b-P4VP(AzoR).

Keywords laser ablation, block copolymers, hydrogen-bond, azobenzene derivatives, supramolecular assembly

1 Introduction

The interaction of high energy lasers with polymers can result in ablation of polymers at irradiated areas [1–11]. Laser ablation is a quick and efficient method to fabricate microstructures and devices on polymers because structures can be generated by a single laser pulse at a time scale of nanosecond or even shorter [1,3–5,10,11]. Ablated structures on polymers show many applications, such as superhydrophobic surfaces [6], multichip modules [7], distributed feedback lasers [4], inkjet printer nozzles [8], and diffractive optical elements [5].

Although laser ablation of polymers is extensively studied and shows many applications, studies on laser ablation of block copolymers (BCPs) are rare [9]. BCPs can form various microphase separated nanostructures [12]. The self-assembly of block copolymers is a promising platform for the fabrication of nanostructured materials and devices [13–20]. We previously reported that BCPs can be hierarchically structured by combining phase separation with laser interference ablation [10]. Shorter length scale structures of the hierarchical structures are phase separated nanostructures and longer length scale structures are interference patterns generated by laser ablation [10]. However, there is a lack of fundamental understanding of laser ablation of block copolymers. Understanding laser ablation of BCPs is helpful for the design of BCPs which can be effectively ablated and patterned. Additionally, lowering ablation thresholds of BCPs is important because low thresholds can increase the ablation rate and save energy. So, it is highly desirable to understand laser ablation of BCPs and decrease ablation thresholds of BCPs.

In this work, we studied the laser ablation of polystyrene-block-poly(4-vinyl pyridine) (PS-b-P4VP) with hydrogen-bonded azobenzene derivatives (AzoR). We found that the ablation threshold of BCP supramolecular assemblies PS-b-P4VP(AzoR) decreases as the concentration of AzoR increases. In PS-b-P4VP(AzoR) with different substituents (R = CN, H, and CH_3), ablation thresholds follow the trend: PS-b-P4VP(AzoCN) < PS-b-P4VP(AzoCH_3) < PS-b-P4VP(AzoH). We showed how chemical structures affect the laser ablation behavior of PS-b-P4VP(AzoR). According to these results, we can effectively fabricate tunable hierarchical structures on BCPs by laser ablation.

Received February 12, 2018; accepted April 10, 2018

E-mails: huangyouju@mpip-mainz.mpg.de (Huang Y), wusi@mpip-mainz.mpg.de (Wu S)

2 Experimental

2.1 Materials

The chemical structures of used materials are shown in Fig. 1. PS-b-P4VP (M_n = 330-b-125 kg·mol^{-1} and PDI = 1.18) was purchased from Polymer Source. The azobenzene derivatives AzoCN and AzoCH$_3$ were synthesized according to our previous work [10,21]. AzoH was purchased from Aldrich.

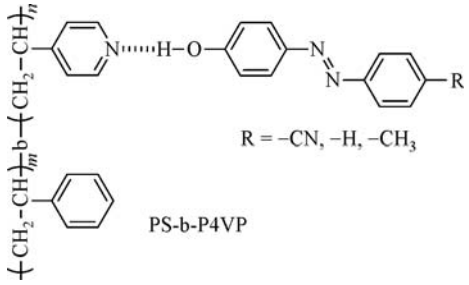

Fig. 1 Chemical structures of used materials. The azo compounds AzoR (R = CN, H, and CH_3) are hydrogen bonded to P4VP blocks of PS-b-P4VP

2.2 Preparation of thin films

PS-b-P4VP and AzoR were dissolved in cyclopentane separately. Solutions of PS-b-P4VP(AzoR)$_x$ were prepared by combining the above two solutions. Here, x denotes the molar ratio of AzoR versus repeat units of P4VP. The mixed solutions were stirred overnight and filtered through a 0.2 μm filter before use. Thin films of PS-b-P4VP (AzoR)$_x$ were prepared by spin-coating. The films had a typical thickness of 200–230 nm. The spin-cast films were dried in an oven under vacuum at room temperature overnight. To induce phase separation, thin films were transferred to a glass container with saturated atmosphere of 1,4-dioxane. The container was completely closed and thin films were kept in the container for 2 days at room temperature.

2.3 Methods

Ultraviolet-visible (UV-vis) absorption spectra were measured on a Perkin-Elmer Lambda 900 UV-vis spectrometer. AFM images were obtained on a Dimension 3100 system using tapping mode. The optical setup for the three-beam interference was reported elsewhere [3,5,10,11]. In brief, a Q-switched Nd:YAG laser at 355 nm with laser pulse duration of 35 ns was used as the light source. The laser beam with pulse energy 1.18 mJ and a diameter of ~1.4 mm was split into three beams with equal intensity to overlap on the sample. The intersecting angle between the interference beams was 5.88°. Interference patterns were fabricated by single pulse irradiation. The intensity distribution of the interference pattern was calculated according to our previous work [3,5,11].

3 Results and discussion

3.1 Effects of the concentration of azobenzene derivatives on laser ablation

It is well known that small molecules with hydrogen bonding donors can be hydrogen-bonded to P4VP blocks of PS-b-P4VP [22–27]. Here, the phenolic group in AzoR is a hydrogen bonding donor (Fig. 1). AzoR can be hydrogen-bonded to P4VP [10,28,29]. The hydrogen bonding between AzoCN and P4VP is proved by infrared spectroscopy (Fig. S1, cf. Electronic Supplementary Material).

Figure 2 shows UV-vis absorption spectra of PS-b-P4VP (AzoCN)$_x$ films with different concentrations of AzoCN. The band at 300–400 nm is the π-π* absorption band of azobenzene groups. The absorption coefficient (α) increases as the concentration of AzoCN increases.

PS-b-P4VP(AzoR)$_x$ forms phase separated nanostructures (Fig. S2) [10]. The schematic model in Fig. 3(a) shows that PS forms the continuous phase and P4VP (AzoR)$_x$ forms dispersed phases. Figure 3(c) shows the hexagonal interference pattern of three beams, which is calculated according to our previous work [3,5,11]. When PS-b-P4VP(AzoR)$_x$ is exposed to interference beams, the polymers at bright interference fringes (high intensity areas) will be ablated. Hierarchical structures with both phase separated nanostructures and interference patterns can be obtained by laser interference ablation (Fig. 3(b)). We will show effects of the concentration of AzoCN on laser ablation.

Figure 4 shows atomic force microscope (AFM) images

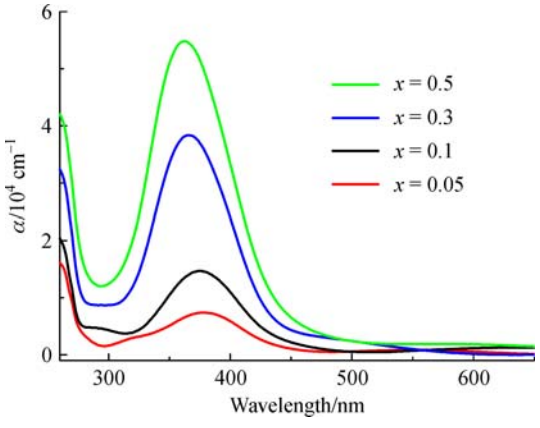

Fig. 2 UV-vis absorption spectra of thin films of PS-b-P4VP (AzoCN)$_x$ (x = 0.05, 0.1, 0.3, and 0.5)

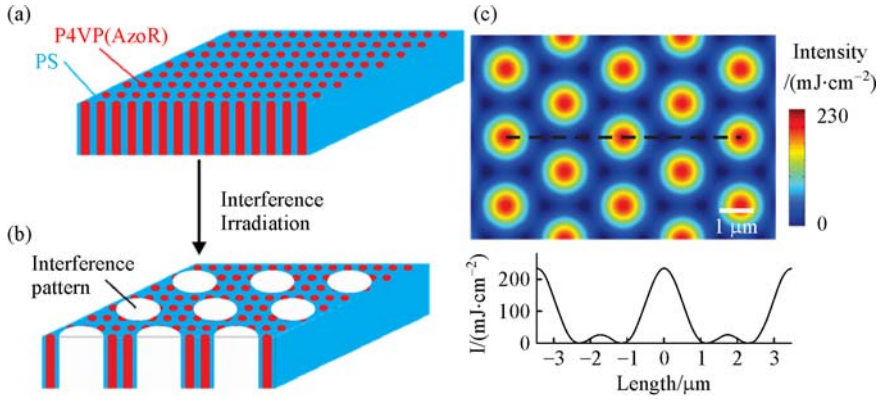

Fig. 3 Schematic models of PS-b-P4VP(AzoR)$_x$ (a) before and (b) after interference irradiation. After irradiation, periodic ablated areas (interference patterns) appear on PS-b-P4VP(AzoR)$_x$. (c) Calculated intensity distribution (top) and profile (bottom) of three beam interference

of PS-b-P4VP(AzoCN)$_x$ (x = 0.05, 0.1, 0.3, and 0.5) after single pulse interference irradiation. All samples form hierarchical structures, which resemble the schematic model in Fig. 3(b). Shorter length scale structures of the hierarchical structures are phase separated nanostructures and longer length scale structures are interference patterns. AFM phase images (insets of Figs. 4(a–d)) clearly show the phase separation between PS and P4VP(AzoCN)$_x$. The average center-to-center distance (period) of nearby P4VP (AzoCN)$_x$ phases increases form ~75 nm (x = 0.05) to ~105 nm (x = 0.5). The period of the interference patterns is ~2 μm. We compared the AFM profiles of PS-b-P4VP (AzoCN)$_x$ with different x (Fig. 4(e)). PS-b-P4VP (AzoCN)$_{0.05}$ forms volcano-like structures, indicating its surface is swelled by laser beams. In the other samples, deep ablated holes are observed. PS-b-P4VP(AzoCN)$_{0.1}$ forms very sharp holes. PS-b-P4VP(AzoCN)$_{0.3}$ and PS-b-P4VP(AzoCN)$_{0.5}$ form deep and wide holes. The depth and diameter of the holes increases as the concentration of AzoCN increases (Fig. 4(f)).

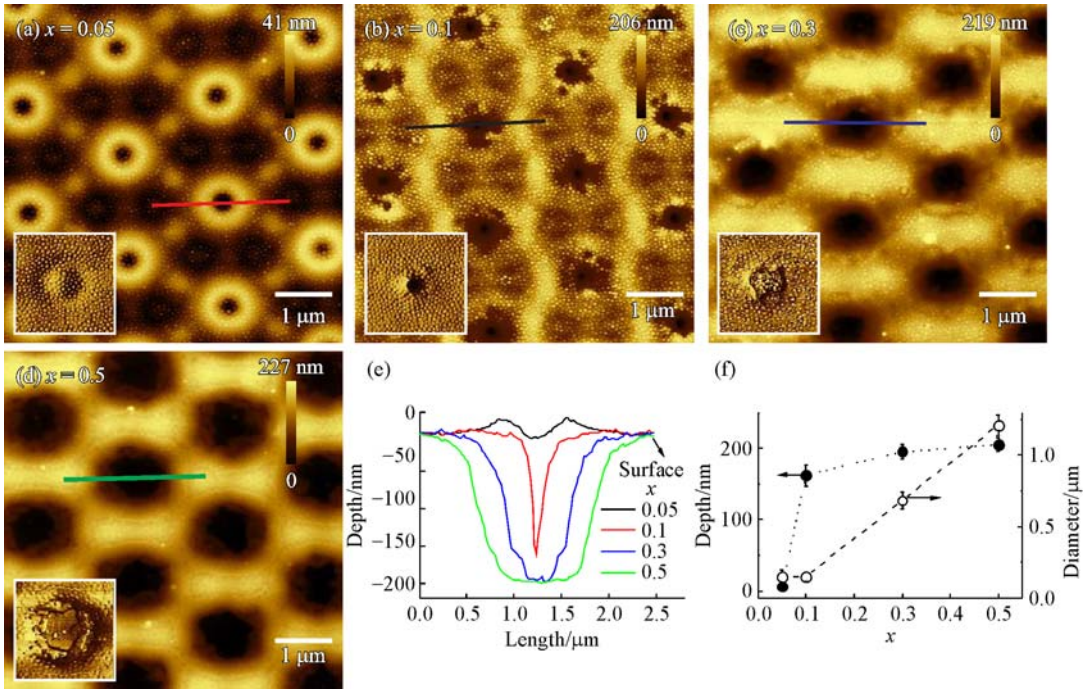

Fig. 4 AFM height images of PS-b-P4VP(AzoCN)$_x$ with different x after exposed to interference beams. (a) x = 0.05, (b) x = 0.1, (c) x = 0.3, and (d) x = 0.5. Insets are AFM phase images, which show that phase separated nanostructures in PS-b-P4VP(AzoCN)$_x$; (e) profiles along the lines in (a)–(d); (f) depths and diameters of the holes generated by interference irradiation. Note: The diameters are measured at half depths of the holes

3.2 Effects of substituents of azobenzene derivatives on laser ablation

We also studied effects of substituents of azobenzene derivatives on laser interference ablation. The hydroxyl group on the para-position of azobenzene is an electron donor (D) [30]. The methyl group (CH_3) of $AzoCH_3$ is also an electron donor. The nitrile group (CN) of AzoCN is an electron acceptor (A). So, AzoH is a D-π molecule, $AzoCH_3$ is a D-π-D molecule, and AzoCN is a D-π-A molecule. These substituents affect the absorption of azo chromophores. Figure 5 shows UV-vis absorption spectra of AzoR in solutions and PS-b-P4VP(AzoR)$_x$ films. The band at 300-400 nm is the characteristic absorption band of azobenzene groups. The bands of $AzoCH_3$ in solution and thin film slightly red-shift compared with those of AzoH. The bands of AzoCN obviously red-shift compared with those of AzoH. These results show that the D-π-D structure slightly affects the absorption of azo chromophores, and D-π-A structure strongly affects the absorption of azo chromophores.

Figure 6 shows AFM images of PS-b-P4VP(AzoH)$_{0.5}$ and PS-b-P4VP($AzoCH_3$)$_{0.5}$ after interference irradiation. They form hierarchical structures with phase separated

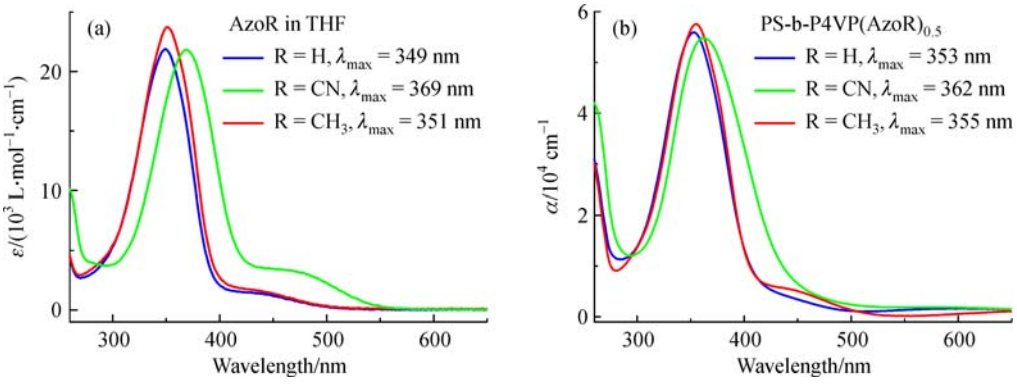

Fig. 5 UV-vis absorption spectra of (a) 10^{-5} mol·L^{-1} AzoR in THF and (b) thin films of PS-b-P4VP(AzoR)$_{0.5}$

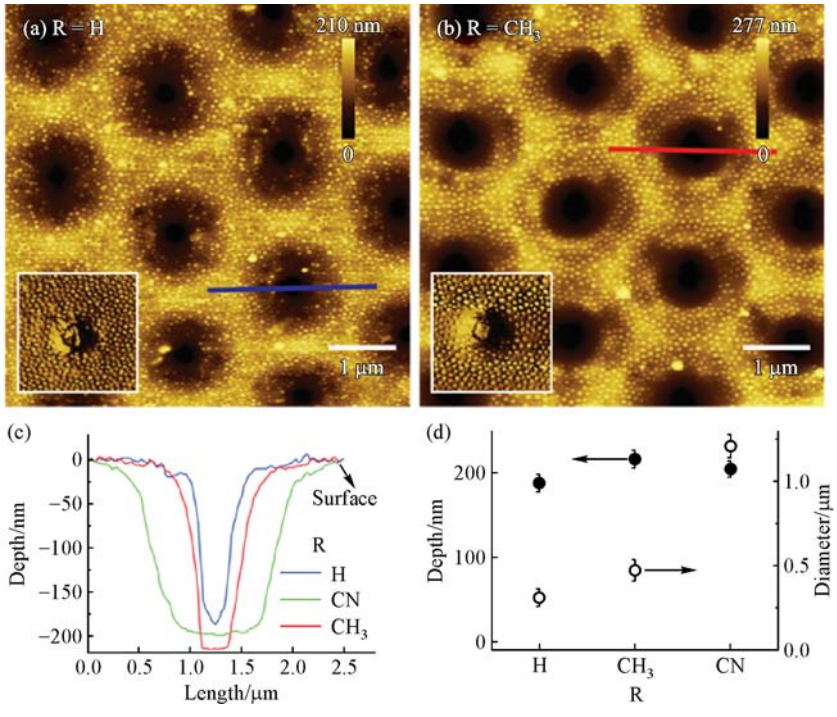

Fig. 6 (a) AFM height images of PS-b-P4VP(AzoH)$_{0.5}$ and (b) PS-b-P4VP($AzoCH_3$)$_{0.5}$ after exposed to interference beams. Insets are AFM phase images of PS-b-P4VP(AzoR)$_{0.5}$. The phase separated nanostructures are clearly visible in the AFM phase images; (c) profiles along the lines in (a), (b), and Fig. 4(d); (d) depths and diameters of the holes generated by interference irradiation. Note: the diameters are measured at half depths of the holes

nanostructures and laser interference patterns. We compared the profiles of PS-b-P4VP(AzoR)$_{0.5}$ (Figs. 6(c) and 6(d)). PS-b-P4VP(AzoH)$_{0.5}$ forms sharp holes. The hole of PS-b-P4VP(AzoCH$_3$)$_{0.5}$ is slightly broader than that of PS-b-P4VP(AzoH)$_{0.5}$. The hole of PS-b-P4VP(AzoCN)$_{0.5}$ is much broader than that of PS-b-P4VP(AzoH)$_{0.5}$. These results indicate that the substituent of AzoR plays an important role on laser ablation.

The mechanism of laser ablation is as follows: When a target is irradiated by a high energy laser, the target absorbs light. Then, the target is heated or decomposed, and subsequent vaporization occurs [1–3,32]. PS-b-P4VP (AzoR)$_x$ is different from normal targets because the light absorber AzoR is in P4VP phases but not homogenously dispersed in the matrix. When PS-b-P4VP (AzoR)$_x$ is exposed to laser beams, AzoR is heated or decomposed. The heat diffuses to hydrogen bonded P4VP chains and nearby PS chains. The heated parts are ablated. P4VP(AzoR) phases are heating centers and the PS phase that does not absorb light obtains heat by thermal diffusion. Considering that the laser pulse duration is 35 ns and thermal diffusivity of PS is in the order of ~10^{-3} $cm^2 \cdot s^{-1}$ [33,34], the heated range of PS during an exposure time of a single pulse is several tens of nanometers near P4VP (AzoR) phases.

The concentration of AzoCN affects the ablation process (Fig. 4). The reason is that AzoCN is the light absorber and the linear absorption coefficient of PS-b-P4VP(AzoCN)$_x$ increases as x increases (Fig. 2 and Table 1). Ablation should be more efficient with more light absorbers. We calculated ablation thresholds of PS-b-P4VP(AzoCN)$_x$ by AFM (Fig. S3). Ablation thresholds of PS-b-P4VP (AzoCN)$_x$ decrease as x increases (Table 1). This result explains why different morphologies are generated on PS-b-P4VP(AzoCN)$_x$ with different x (Fig. 4).

Table 1 Linear absorption coefficients (α) at 355 nm and ablation thresholds of PS-b-P4VP(AzoR)$_x$

Sample	α/10^4 cm^{-1}	Threshold/(mJ·cm^{-2})
PS-b-P4VP(AzoCN)$_{0.05}$	0.57	\
PS-b-P4VP(AzoCN)$_{0.3}$	3.61	81±10
PS-b-P4VP(AzoCN)$_{0.5}$	5.35	47±10
PS-b-P4VP(AzoH)$_{0.5}$	5.58	208±10
PS-b-P4VP(AzoCH$_3$)$_{0.5}$	5.75	165±10

Substituents of AzoR also affect the interference ablation (Fig. 6). As shown in Table 1, the linear absorption coefficients of PS-b-P4VP(AzoR)$_{0.5}$ (R = H, CN, and CH$_3$) are nearly the same, but their ablation thresholds are quite different. This result indicates that not only the linear absorption coefficient affects laser ablation. It is well known that azo dyes show nonlinear absorption, i.e., the absorption coefficient of an azo dye is strongly dependent on the laser intensity [30,35,36]. D-π-D and D-π-A molecules usually show better nonlinear absorption [30,35–38]. AzoCH$_3$ and AzoCN are D-π-D and D-π-A molecules, respectively, which can more efficiently absorb light of high energy lasers. So, different ablation thresholds of PS-b-P4VP(AzoR)$_{0.5}$ (R = H, CN, and CH$_3$) are due to different chemical structures of AzoR.

4 Conclusions

Both the concentration and the substituent of AzoR dominate the laser ablation of PS-b-P4VP(AzoR)$_x$. The ablation threshold decreases as the concentration of azobenzene derivatives increases. This result is because the linear absorption coefficient increases as the concentration of azobenzene derivatives increases. The samples with different substituents (PS-b-P4VP(AzoR)$_{0.5}$) have nearly the same linear absorption coefficient, but their ablation thresholds are quite different. Ablation thresholds follow the trend: PS-b-P4VP(AzoCN)$_{0.5}$ < PS-b-P4VP (AzoCH$_3$)$_{0.5}$ < PS-b-P4VP(AzoH)$_{0.5}$. This trend is due to the D-π-A and D-π-D structures of AzoCN and AzoCH$_3$, respectively. These results are helpful for the design of BCP systems with low ablation thresholds, which can be effectively structured at low laser intensities.

Tunable hierarchical structures can be fabricated by laser interference ablation of BCPs. Phase separated nanostructures are tunable by changing the composition of BCPs [10] or the concentration of azobenzene derivatives (insets of Fig. 4). Interferences patterns are tunable by changing interference conditions [10], concentration of azobenzene derivatives (Fig. 4), or substituents of azobenzene derivatives (Fig. 6). We observed that hierarchical structures on PS-b-P4VP(AzoR)$_x$ show brilliant structural colors. The hierarchical structures show potential applications as photonic materials.

Acknowledgements This study was supported by the joint program of the Max Planck Society and the Chinese Academy of Sciences. We thank Prof. C. Bubeck for helpful discussions. Open access funding provided by Max Planck Society.

Electronic Supplementary Material Supplementary material is available in the online version of this article at https://doi.org/10.1007/s11705-018-1735-6 and is accessible for authorized users.

References

1. Lippert T, Dickinson J T. Chemical and spectroscopic aspects of polymer ablation: Special features and novel directions. Chemical

Reviews, 2003, 103(2): 453–486
2. Weis P, Wu S. Light-switchable azobenzene-containing macromolecules: From UV to near infrared. Macromolecular Rapid Communications, 2018, 39(1): 1700220
3. Huang J, Wu S, Beckemper S, Gillner A, Zhang Q, Wang K. All-optical fabrication of ellipsoidal caps on azobenzene functional polymers. Optics Letters, 2010, 35(16): 2711–2713
4. Zhai T, Zhang X, Pang Z, Dou F. Direct writing of polymer lasers using interference ablation. Advanced Materials, 2011, 23(16): 1860–1864
5. Huang J T, Beckemper S, Gillner A, Wang K Y. Tunable surface texturing by polarization-controlled three-beam interference. Journal of Micromechanics and Microengineering, 2010, 20(9): 095004
6. Wohl C J, Belcher M A, Chen L, Connell J W. Laser ablative patterning of copoly(imide siloxane)s generating superhydrophobic surfaces. Langmuir, 2010, 26(13): 11469–11478
7. Patel R S, Wassick T A. Laser processes for multichip module's high density multilevel thin film packaging. Laser Applications in Microelectronic and Optoelectronic Manufacturing II, 1997, 2991: 217–223
8. Aoki H. Laser processing method to form an ink jet nozzle plate. US Patent, 1998
9. Weis P, Tian W, Wu S. Photoinduced liquefaction of azobenzene-containing polymers. Chemistry, 2018, 24(25): 6494–6505
10. Wu S, Huang J T, Beckemper S, Gillner A, Wang K Y, Bubeck C. Block copolymer supramolecular assemblies hierarchically structured by three-beam interference laser ablation. Journal of Materials Chemistry, 2012, 22(11): 4989–4995
11. Huang J, Beckemper S, Wu S, Shen J, Zhang Q, Wang K, Gillner A. Light driving force for surface patterning on azobenzene-containing polymers. Physical Chemistry Chemical Physics, 2011, 13(36): 16150–16158
12. Bates F S, Fredrickson G H. Block copolymer thermodynamics: theory and experiment. Annual Review of Physical Chemistry, 1990, 41(1): 525–557
13. Bang J, Jeong U, Ryu Y, Russell T P, Hawker C J. Block copolymer nanolithography: Translation of molecular level control to nanoscale patterns. Advanced Materials, 2009, 21(47): 4769–4792
14. Cheng J Y, Ross C A, Smith H I, Thomas E L. Templated self-assembly of block copolymers: Top-down helps bottom-up. Advanced Materials, 2006, 18(19): 2505–2521
15. Zhou H, Xue C, Weis P, Suzuki Y, Huang S, Koynov K, Auernhammer G K, Berger R, Butt H J, Wu S. Photoswitching of glass transition temperatures of azobenzene-containing polymers induces reversible solid-to-liquid transitions. Nature Chemistry, 2017, 9(2): 145–151
16. Guo C H, Lee Y, Lin Y H, Strzalka J, Wang C, Hexemer A, Jaye C, Fischer D A, Verduzco R, Wang Q, Gomez E D. Photovoltaic performance of block copolymer devices is independent of the crystalline texture in the active layer. Macromolecules, 2016, 49 (12): 4599–4608
17. Hung C C, Chiu Y C, Wu H C, Lu C, Bouilhac C, Otsuka I, Halila S, Borsali R, Tung S H, Chen W C. Conception of stretchable resistive memory devices based on nanostructure-controlled carbohydrate-block-polyisoprene block copolymers. Advanced Functional Materials, 2017, 27(13): 1606161
18. Mitchell V D, Gann E, Huettner S, Singh C R, Subbiah J, Thomsen L, McNeill C R, Thelakkat M, Jones D J. Morphological and device evaluation of an amphiphilic block copolymer for organic photovoltaic applications. Macromolecules, 2017, 50(13): 4942–4951
19. Yoo H G, Byun M, Jeong C K, Lee K J. Performance enhancement of electronic and energy devices via block copolymer self-assembly. Advanced Materials, 2015, 27(27): 3982–3998
20. Wang J, Wu B, Li S, Sinawang G, Wang X, He Y. Synthesis and characterization of photoprocessable lignin-based azo bolymer. ACS Sustainable Chemistry & Engineering, 2016, 4(7): 4036–4042
21. Wu S, Duan S Y, Lei Z Y, Su W, Zhang Z S, Wang K Y, Zhang Q J. Supramolecular bisazopolymers exhibiting enhanced photoinduced birefringence and enhanced stability of birefringence for four-dimensional optical recording. Journal of Materials Chemistry, 2010, 20(25): 5202–5209
22. Ikkala O, ten Brinke G. Functional materials based on self-assembly of polymeric supramolecules. Science, 2002, 295(5564): 2407–2409
23. Kuila B K, Stamm M. Block copolymer-small molecule supramolecular assembly in thin film: A novel tool for surface patterning of different functional nanomaterials. Journal of Materials Chemistry, 2011, 21(37): 14127–14134
24. Zhao Y, Thorkelsson K, Mastroianni A J, Schilling T, Luther J M, Rancatore B J, Matsunaga K, Jinnai H, Wu Y, Poulsen D, Fréchet J M, Alivisatos A P, Xu T. Small-molecule-directed nanoparticle assembly towards stimuli-responsive nanocomposites. Nature Materials, 2009, 8(12): 979–985
25. Roland S, Gaspard D, Prud'homme R E, Bazuin C G. Morphology evolution in slowly dip-coated supramolecular PS-b-P4VP thin films. Macromolecules, 2012, 45(13): 5463–5476
26. Soininen A J, Tanionou I, ten Brummelhuis N, Schlaad H, Hadjichristidis N, Ikkala O, Raula J, Mezzenga R, Ruokolainen J. Hierarchical structures in lamellar hydrogen bonded LC side chain diblock copolymers. Macromolecules, 2012, 45(17): 7091–7097
27. Huang W H, Chen P Y, Tung S H. Effects of annealing solvents on the morphology of block copolymer-based supramolecular thin films. Macromolecules, 2012, 45(3): 1562–1569
28. de Wit J, van Ekenstein G A, Polushkin E, Kvashnina K, Bras W, Ikkala O, ten Brinke G. Self-assembled poly(4-vinylpyridine)—surfactant systems using alkyl and alkoxy phenylazophenols. Macromolecules, 2008, 41(12): 4200–4204
29. Priimagi A, Vapaavuori J, Rodriguez F J, Faul C F J, Heino M T, Ikkala O, Kauranen M, Kaivola M. Hydrogen-bonded polymer-azobenzene complexes: Enhanced photoinduced birefringence with high temporal stability through interplay of intermolecular interactions. Chemistry of Materials, 2008, 20(20): 6358–6363
30. Liu Z Y, Lu G Y, Ma J. Tuning the absorption spectra and nonlinear optical properties of D-pi-A azobenzene derivatives by changing the dipole moment and conjugation length: A theoretical study. Journal of Physical Organic Chemistry, 2011, 24(7): 568–577
31. Ki H, Mohanty P S, Mazumder J. Modelling of high-density laser-material interaction using fast level set method. Journal of Physics. D, Applied Physics, 2001, 34(3): 364–372
32. Martukanitz R P. A critical review of laser beam welding. In: Schriempf J T, ed. Critical Review: Industrial Lasers and

Applications. Bellingham: Spie-Int Soc Optical Engineering, 2005, 11–24

33. Hattori M. Thermal diffusivety of some linear polymers. Kolloid-Zeitschrift and Zeitschrift Fur Polymere, 1965, 202(1): 11–14
34. Morikawa J, Kobayahi A, Hashimoto T. Thermal diffusivity in a binary mixture of poly(phenylene oxide) and polystyrene. Thermochimica Acta, 1995, 267: 289–296
35. Yesodha S K, Sadashiva Pillai C K, Tsutsumi N. Stable polymeric materials for nonlinear optics: A review based on azobenzene systems. Progress in Polymer Science, 2004, 29(1): 45–74
36. Liu R, Li Y H, Chang J, Xiao Q, Zhu H J, Sun W F. Photophysics and nonlinear absorption of 4,4′-diethynylazobenzene derivatives terminally capped with substituted aromatic rings. Journal of Photochemistry and Photobiology A Chemistry, 2012, 239: 47–54
37. Tian L, Hu Z J, Shi P F, Zhou H P, Wu H Y, Tian Y P, Zhou Y F, Tao X T, Jiang M H. Synthesis and two-photon optical characterization of D-pi-D type schiff bases. Journal of Luminescence, 2007, 127(2): 423–430
38. Fitilis I, Fakis M, Polyzos I, Giannetas V, Persephonis P, Mikroyannidis J. Strong two photon absorption and photophysical properties of symmetrical chromophores with electron accepting edge substituents. Journal of Physical Chemistry A, 2008, 112(21): 4742–4748